Alq J Sci. 2025;1(2):157-171
https://doi.org/10.69667/ajs.25205
Alqalam Journal of Science
مجلـــة القلم للعلـوم
https://alqalam.utripoli.edu.ly/index.php/AR

Original article

Raman Light Scattering Study of the Isotopic Construction Effects on the Lattice properties -TO and LO Phonon modes- of CuCl

Nadir Driza*, Ola Mohammed, Asma Elgade

Department of Physics, Faculty of Arts and Sciences, Elmarj, University of Benghazi, Benghazi, Libya
Corresponding E-mail: *nadir.driza@uob.edu.ly*

Abstract
This work expands on our research on isotope effects on phonons to include compound semiconductors. In this article, we concentrate our study on the variation of the lattice properties, such as lattice dynamics and electronic structure, due to the effects of isotope substitution on the CuCl Raman spectra. We fulfilled that by examining 35Cl, 37Cl, 63Cu, and 65Cu. Unlike elemental semiconductors, compounds whose constituents are isotopically substituted have a substantial dependence on the phonon branch and wave vector q for changes in phonon frequencies and atomic displacements. In the case of CuCl, the substitution of heavy or light atoms has distinct effects on the acoustic and visual branches of the phonon dispersion relations. The significant mass difference between copper and chlorine causes the eigenvectors of the acoustic vibrations to be dominated by copper displacements, while the optic vibrations are dominated by chlorine displacements. Consequently, the phonon frequencies in the visual and acoustic branches can be altered nearly independently, especially at the X point, by employing isotope replacement. At low temperatures, this enables us to examine the effectiveness of the anharmonic decay channels of Γ-point optical phonons into lower-lying acoustic bands.
Keywords. Isotopic, Lattice Properties, TO Phonon Mode, LO Phonon Mode, Raman Light Scattering.

Introduction

Isotopes are atoms with the same number of protons and electrons but a different number of neutrons. Isotopes differ in mass but are chemically identical. Early theoretical works have established that only properties dependent on nuclear mass are altered in isotopes. The most obvious instance of such dependence is the mass-dependent effect on the harmonic lattice vibrational frequency, which is represented as $1/\sqrt{m}$. Isotope-dependent properties also include properties that are affected by changes in unit cell volume, atomic hopping mobility, and anharmonicities—for example, thermal conductivity, thermal expansion, melting temperature, nuclear magnetic resonance, and superconducting phase transition temperature. The electronic band structures were once believed to remain identical in isotopes under such changes. However, this belief has been justified only by atomic-spectra data. Evidence has revealed that in the case of molecular spectra, the effect of mass involves differences between isotopes through the mechanism of electron–phonon coupling [Watanabe, 2009, P1426] [Kragh, 2012, P179]. The presence of an isotope effect is an effective indicator of phonon-mediated superconductivity in materials and constitutes support for the Bardeen–Cooper–Schrieffer (BCS) theory of superconductivity [Gweon, 2004, P187, P188] [Cheng, 2017, P1-4], [Hodovanets, 2013, P1748-1753] [Bud'ko, 2001, P1877, P1878].
The ionicity of copper chloride is f_i = 0.75. Of all the binary compounds that crystallize in the zincblende structure at room temperature and pressure, it is therefore one of the semiconductors that shows the highest ionicity [Phillips, 1970, P332, P346] [Alhaddad, 2025, P9] [Göbel, 1997, P210]. The six-fold coordinated rock-salt structure is preferred above a critical value of f_i [Ono, 2020, P1], which is f_c = 0.785(10). The physical properties of CuCl, which are near phase transitions, show several peculiarities that have been thoroughly studied. For example, the linear expansion coefficient at low temperatures is strongly negative, which is associated with the negative mode-Grüneisen parameters of the acoustic branches at the zone edges. A strongly anharmonic lattice potential has been linked to the expansion coefficient and the tiny elastic shear constants c_{44} and $c_s = (c_{11} - c_{12})/2$, which decrease with increasing hydrostatic pressure [Varshney, 2016, P1, P2]. The inverted spin-orbit splitting in CuCl [Hodges, 2007, P1] and changes in the band gap with isotope substitution [Yu, 2004, P1-P4] show that the admixture of the copper d electrons to the chlorine p levels is essential for the valence band structure [Quevedo, 2020, P10]. Even at low temperatures, the mean square atomic displacement of Cu in CuCl is substantial, and it keeps rising as the temperature rises. Though not as noticeable, CuBr and CuCl exhibit comparable behavior [Wang, 2023, P1,2].
The mean square atomic displacement of Cu in CuCl is large even at low temperature, and it continues to increase with increasing temperature. CuBr and Cu2 show a similar behavior, although not as pronounced [Wang, 2023, P1,2]. There are three models to describe the large mean square displacements. Those models have been considered as the following: first model is isotopic thermal vibrations of copper atoms within a harmonic model [Majzlan, 2023, P1-P3], second model describes displacements along the tetrahedral axes as a result of asymmetric anharmonic thermal vibrations [Aree, 2022, P1], and the third model clarifies a

Received*: 02-07-2025 -* ***Accepted****: 01-09-2025 -* ***Published****: 10-09-2025*

Alq J Sci. 2025;1(2):157-171
https://doi.org/10.69667/ajs.25205
Alqalam Journal of Science
مجلـــة القلم للعلـوم
https://alqalam.utripoli.edu.ly/index.php/AR

statistical occupation of metastable positions displaced from the ideal lattice site along the [111] axes [Wang, 2023, P1]. It is clearly shown that the harmonic model is not consistent with their room temperature neutron diffraction data. In contrast, the anharmonic lattice potential model, just like the disorder model refined by a temperature-dependent metastable off-center position, can explain the Bragg peak intensities observed in neutron diffraction. Schreurs et al. have examined the diffuse neutron scattering background and found that 50 to 70% of it is elastic [Sakata, 1974, P655-P661]. From this, they concluded that a model including correlated displacements from the ideal zincblende lattice site must be developed [Schreurs, 1976, P618]. For subsequent powder neutron investigations, however, an anharmonic lattice potential was sufficient to account for the data [Lan, 2014, P1, 2]. It should be noted that all of the above data were obtained at or substantially above room temperature.

Copper halides, a family of chemical compounds, are notable for their ability to conduct electricity. A prime example is copper chloride (CuCl), which exhibits a fascinating change in conductivity with rising temperature. At a temperature of 400 K, the conductivity of CuCl is a modest σ = 4.5 x 10^{-6} $\Omega^{-1}cm^{-1}$. However, as the material is heated, its conductivity increases sharply, reaching 0.10 $\Omega^{-1}cm^{-1}$ at 700 K. Around this temperature, a significant change occurs: the crystal structure of the CuCl transforms. Interestingly, while other copper halides like copper bromide and copper iodide become "superionic conductors" under normal pressure, CuCl does not. To achieve a similar state of high conductivity, CuCl needs to be put under extreme conditions. At approximately 680 K and a very high pressure of 1 GPa, it transforms a new cubic structure. In this structure, the chlorine atoms form a fixed, stable lattice, while the copper ions become highly mobile, distributed randomly within the gaps of the chlorine framework. This disordered state of the copper ions is what allows for the material's increased electrical conductivity. Its high cationic conductivity, roughly 10 Ω^{-1} cm^{-1}, characterizes the superionic phase of CuCl. With a modest temperature dependence, this conductivity approaches levels that are characteristic of molten salts [Sekkal, 1998, P1293]. An "melting" of the cationic sublattice is shown by the latent temperatures linked to the transition to this superionic state. A preferential conduction path for the cation within the superionic phase of copper halides is along the [111] direction, according to experimental data from EXAFS measurements [Boyce, 1981, P1]. Furthermore, Schneider et al. [Schneider, 1992, P3196] have identified local tunneling of muonium between tetrahedral interstices, each of which has four nearby copper atoms.

The ac magnetic susceptibility of quickly warmed materials likewise showed diamagnetic anomalies above 90 K throughout a temperature range of 10 to 20 K [Stegemann, 2019, P1] [Lefkowitz, 1979, P4506]. Their size and temperature range varied from sample to sample, but the anomalies were reproducible for a given sample. The observed diamagnetic anomaly was thought to be a hint of the Meissner effect in superconducting materials. However, the observed anomalies are still poorly understood because superconductivity in CuCl could not be verified [Lefkowitz, 1979, P4506].

The Raman spectrum of CuCl is unusual, even at 5 K. Instead of the single TO phonon peak expected for this type of material, it has a standard LO phonon peak (~209 cm^{-1}) and a broad structure in the TO region with at least two additional peaks (145-175 cm^{-1}) [Ulrich, 1999, P351]. All three peaks are broad but remain stable at higher temperatures. We will be using the Fukumoto et al. notation to identify them [Park, 1996, P2314], [Fukumoto, 1976, P349]. For instance, in Fig. 1, we display the Raman spectra of multiple isotopically changed CuCl samples at 5 K. As one moves from the bottom to the top of the spectrum, the lowered mass u increases. The LO phonon shifts monotonically to smaller frequencies in accordance with that. On the other hand, it is already evident that the isotopic composition significantly influences the form of the TO structure line, namely, the fact that the $TO(\gamma)$ The peak does not change monotonically as the mass changes. This raises the prospect that the nature of the TO structure can be elucidated by the examination of the changes in line form upon isotope substitution.

Received*: 02-07-2025 -* ***Accepted****: 01-09-2025 -* ***Published****: 10-09-2025*

Alq J Sci. 2025;1(2):157-171
https://doi.org/10.69667/ajs.25205
Alqalam Journal of Science
مجلـــة القلم للعلـوم
https://alqalam.utripoli.edu.ly/index.php/AR

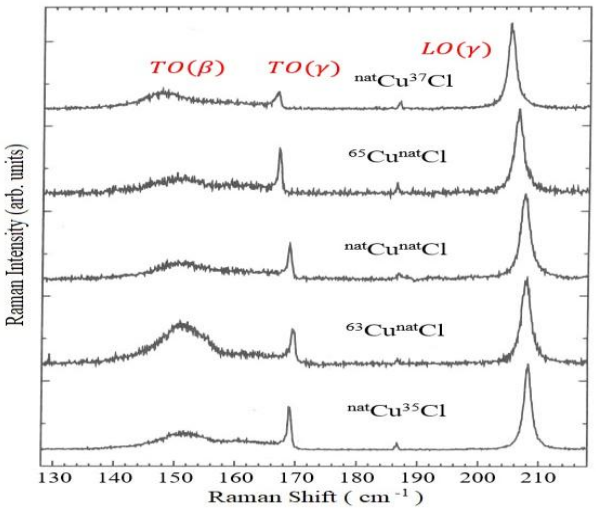

Fig1. Raman Spectra of isotopically modified CuCl at 5 K. The reduced mass μ increases from the bottom to the top. The LO phonon amplitude was normalized to one for all spectra. A strong isotope dependence of the TO phonon position and, in particular, the intensity relative to that of the LO phonon is apparent.

The zone center is not the only location where the two-peak TO structure appears. It was demonstrated to extend into the Brillouin zone using inelastic neutron scattering. It was detected at least 0.2 r.l.u. from the Γ point along the three high symmetry directions Δ, Σ, and Λ.

A number of departures from the typical behavior have been found when comparing the temperature dependence of the CuCl Raman spectra to that seen for other zincblende semiconducting compounds: Because of the negative thermal expansion coefficients below 100K, the LO phonon frequency increases from 0 to 90K and only drops above 90K [Vaccari, 2007, P1]. While the $TO(\gamma)$ and $TO(\beta)$ modes' frequencies fall monotonically as the temperature rises, the $TO(\beta)$ modes' temperature dependency is surprisingly considerable, measuring roughly 35 cm^{-1} between 0 and 300 K [Potts, 1974, P2712]. Unlike the $TO(\beta)$ mode, which seems to correspond to a first-order Raman line, the temperature dependence of the scattering intensity of the $TO(\gamma)$ peak is incompatible with a one-phonon or two-phonon Bose-Einstein factor [21, Potts, 1974, P2714]. However, considering the mean of the $TO(\gamma)$ and $TO(\beta)$ frequencies, the temperature dependence of the integrated total intensity of the TO structure is likewise consistent with what would be predicted for a first-order Raman process.

There are two possible explanations for the abnormal TO structure: First, a Fermi resonance that repelled the optical phonon out of a two-phonon combination band has been used to describe the anomalous TO spectrum of CuCl [Krauzman, 1974, P529] [Ulrich, 1999, P351, P354]. Conversely, a method has been used to determine how third- and fourth-order anharmonic coupling causes a two-phonon resonance to hybridize with single-phonon states [Pang, 2024, P1] [Behera, 1981, P528, P529]. Third-order anharmonic coupling is adequate to explain both peaks of the TO phonon structure, according to further extensive lattice dynamical simulations [Hattori, 2010, P10, P12].

We present a model computation in Fig.2 that is comparable to the textbook case put out by Shand et al. [Shand, 1976, P4641, P4643]. They have assumed an elliptical density of states. By accounting for cubic and quartic factors in the anharmonic interaction, they have arrived at a broadening $\Gamma(\omega)$ that is comparable to the one seen in Fig. 2 (b). The line shape derived from these two values is displayed in Fig. 2 (c); the frequency-dependent shift Δ(ω) represents the Kramers-Kronig transform of $\Gamma(\omega)$. However, because of the very narrow pressure range examined, predictions for changes in the line shape—that is, changes in the frequencies of $TO(\gamma)$ and $TO(\beta)$ and their intensities—was not conclusive when applying hydrostatic pressure [Shand, 1976, P4643]. Additionally, within the formalism of Ruvalds and Zawadowski [Ruvalds, 1970, P1172-1174], their two-phonon density of states is a model function that is purposefully created to produce the desired line shape. In other words, while an elliptical two-phonon density of states may be a good model, it is only a rough approximation to a realistic one, as we shall see.

Received*: 02-07-2025 -* ***Accepted****: 01-09-2025 -* ***Published****: 10-09-2025*

Alq J Sci. 2025;1(2):157-171
https://doi.org/10.69667/ajs.25205
Alqalam Journal of Science
مجلـــة القلم للعلـوم
https://alqalam.utripoli.edu.ly/index.php/AR

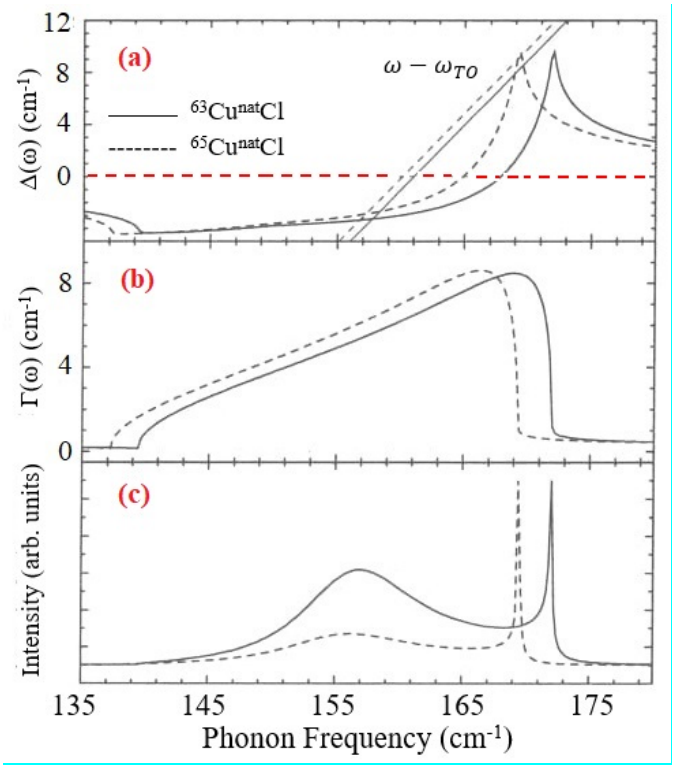

Figure 2. Simulation of the CuCl TO structure. Full line $^{63}Cu^{nat}Cl$, dashed line: $^{65}Cu^{nat}Cl$

Nevertheless, this may be a suitable point to discuss briefly in which way isotope effects have to be taken into account within the Krauzman model. Since the two-phonon density of states is dominated by copper vibrations in this frequency regime, we scale the broadening $\Gamma(\omega)$ by the full copper isotope effect, i.e.,

$$\omega = \sqrt{63/65}\ \omega_{63} = 0.984495\ \omega_{63}.$$

The aforementioned connection causes a somewhat lesser shift in the Γ low-frequency edge compared to its high-frequency edge. For $^{65}Cu^{nat}Cl$, the broadening is somewhat more than that achieved for $^{65}Cu^{nat}Cl$, however, since the total number of two-phonon states must be preserved. The generated spectra show sites of high intensities for which the shift Δ(ω) in Fig. 2 (a) is closest to or intersected by the straight line $(\omega - \omega_{TO})$ The model spectra in Fig.2 (c) are compared to the real spectra in Fig. 1, and we can easily see that the isotope replacement in this model produces the right patterns in shifts and even relative intensities of $TO(\gamma)$ and $TO(\beta)$

However, a number of disorder theories have also been put out to explain the TO structure, in which a significant portion of the Cu atoms are situated at non-ideal lattice locations, resulting in the emergence of extra (local) vibrational modes [Ulrich, 1999, P351, P353]. Cu displacements from the typical zincblende sites are caused by secondary minima in the lattice potential in these models, which are attributed to the large anharmonicity [Göbel, 1997, P211].

The findings of first-principles calculations on structural abnormalities in the Cu halides have recently been supported by references to off-center models. As the copper atom is moved along the [111] axis in an antibonding direction, all-electron density functional theory has been used to get an extra local minimum in the total energy of a 16-atom CuCl supercell [Wei, 1993, P1640, P1641] [Pham, 2020, P2972]. It has been found that the development of a complex of four Cu off-center atoms further reduces the total energy of CuCl for a bigger supercell [Wang, 2023, P1]. They suggest that these complexes may give rise to local modes and link them to the anomalous TO phonon spectrum.

Here, we demonstrate that the Fermi resonance scenario provides a quantitative explanation for the complex variations in the Raman spectra derived from CuCl samples with changed isotopic composition (see Fig. 1) [Serrano, 2002, P1]. A detailed comparison is made between the line shifts, linewidth changes, and intensity ratio changes with isotope replacement. It should be noted that the TO structure may be explained without using a second set of optical phonons [Göbel, 1996, P2591] [Park, 1996, P2592]. Vibrations resulting from the suggested disorder in the material are responsible for this second phonon set. Our data, however, qualitatively differ from the off-center model's predictions.

Received*: 02-07-2025 -* ***Accepted****: 01-09-2025 -* ***Published****: 10-09-2025*

Alq J Sci. 2025;1(2):157-171
https://doi.org/10.69667/ajs.25205
Alqalam Journal of Science
مجلـــة القلم للعلـوم
https://alqalam.utripoli.edu.ly/index.php/AR

Sample Preparation

Two distinct methods were employed for sample preparation. A portion of the samples was synthesized using the Pulsed Laser Deposition (PLD) technique. The remaining samples were produced by heating copper (Cu) metal, with a desired isotopic composition, in a flowing hydrogen chloride (HCl) gas atmosphere.
Natural copper and chlorine each possess two stable isotopes: ^{63}Cu: 71.3%, ^{65}Cu: 28.7%, ^{35}Cl: 78.4%, and ^{37}Cl: 21.6%, respectively. The elemental precursors utilized for sample growth were isotopically pure (99.5%), with the exception of the enriched ^{37}Cl, which contained approximately 9% of ^{35}Cl as quantified by mass spectroscopy. To mitigate potential artifacts arising from variations in chemical impurities and crystalline quality, samples from independent sources were investigated, and their Raman spectra for identical isotopic compositions were confirmed to coincide. The prepared samples were typically presented as platelets, exhibiting a surface area up to 10 mm^2 and a thickness of less than 0.1 mm. X-ray diffraction (XRD) analysis confirmed the samples' surfaces possessed a (111) crystallographic orientation. For samples derived from isotopically pure HCl, initial reaction products underwent purification via two successive sublimations under vacuum, followed by a zone melting process. Subsequent growth of the platelet samples was achieved using a closed-tube transport method employing a hydrogen (H_2) atmosphere.

Raman Spectroscopy

Raman spectra were excited using a Kr-ion laser operating at a wavelength of 406 nm with a power output ranging below 10 mW to avoid heating of the sample. Although copper (I) chloride (CuCl) is transparent at this wavelength, its proximity to the material's bandgap induces resonance effects, significantly enhancing scattering efficiency and enabling high-resolution measurements. To assess for potential line shape distortions or shifts attributable to these resonance effects, additional laser lines (514 nm and 647 nm) were also employed. The scattered light was dispersed by a triple monochromator setup is crucial because two of them are positioned back-to-back to block off stray light, while the third one separates the Raman signal from the laser light, where the focal length (f) was 0.75 m. Spectra were recorded in a backscattering geometry from the [111] surface using single-photon counting. Samples were cryogenically cooled to 5 K by immersion in superfluid helium, with meticulous care taken to minimize sample heating during measurements. Calibration of the spectra was performed against nearby laser plasma lines.

Results and Discussion

The eigenvectors have a significant influence on the variations in the phonon frequencies when various atoms in the unit cell are isotopically swapped.
Mode eigenvectors for the two coupled E2 phonons in wurtzite CdS and GaN may be found using isotope substitution.
[Lin, 2019, P400], [Zhang, 1998, P9716-P9718], [Zhang, 1997, P14399, P14402]. According to the harmonic approximation, the inverse square root of the decreased mass ($\omega \sim 1/\sqrt{\mu}$, $\mu^{-1} = m_{cation}^{-1} + m_{anion}^{-1}$) determines the optical zone center phonon frequencies of zincblende compounds. Together with the sublattice mass variance parameter $g(k)$, which describes the isotope mass variations on the corresponding sublattice of the zincblende sample, we have included the reduced masses of our samples for convenience in Table I. It is provided by

$$g(k) = \sum_i c_i \left(\frac{\bar{m} - m_i}{\bar{m}}\right)^2$$

Here c_i denotes the concentrations of either the cation or anion isotopes i of the respective sublattice. The average mass of the sublattice overline $\bar{m}$ and the isotope mass is denoted by m_i. These mass fluctuations perturb the translational invariance and soften the q conservation rule of crystal momentum, giving rise to elastic disorder-induced scattering of phonons [Lindsay, 2013, P2] [Asen-Palmer, 1997, P9431]. This effect vanishes in isotopically pure samples.

Received: *02-07-2025* - ***Accepted***: *01-09-2025* - ***Published***: *10-09-2025*

Alq J Sci. 2025;1(2):157-171
https://doi.org/10.69667/ajs.25205
Alqalam Journal of Science
مجلـــة القلم للعلـوم
https://alqalam.utripoli.edu.ly/index.php/AR

Table 1. Sublattice mass variance $g(k)$ and reduced mass u in [10^{-4}] $LO(\gamma)$, $LO(\gamma)$, and $TO(\gamma)$ units, Raman linewidths, and frequencies. Several isotopically modified CuCl samples at T = 2K were measured for gamma $\Gamma_{LO(\gamma)}$ (FWHM) in [cm^{-1}] units. The linewidth has been adjusted to account for the resolution of the spectrometer. The mean square deviation of many measurements represents the mistakes.

Sample	μ[amu]	g_{Cu}	g_{Cl}	$\omega_{LO(\gamma)}$	$\Gamma_{LO(\gamma)}$	$\omega_{TO(\gamma)}$	$\omega_{TO(\beta)}$
$^{63}Cu^{35}Cl$[a]	20.78	0	0	210.00	1.62	169.54	153.8
$^{nat}Cu^{35}Cl$	20.69	2.1	0	209.45	1.30	167.93	153.6
$^{63}Cu^{nat}Cl$	20.74	0	5.8	208.98	1.69	168.51	153.2
$^{65}Cu^{35}Cl$[a]	20.82	0	0	208.88	1.61	166.72	152.5
$^{nat}Cu^{nat}Cl$	20.77	2.1	5.8	208.81	1.70	167.87	152.7
$^{65}Cu^{nat}Cl$	20.89	0	5.8	207.79	1.62	166.65	152.1
$^{nat}Cu^{37}Cl$[b]	21.53	2.1	2.9	206.67	1.43	167.36	152.9

(a) Data were taken at T = 5 K; samples have different orientations and were grown by a different process. (b) The Cl-compound contains about 9% ^{35}Cl.

The isotopically adjusted CuCl's $LO(\gamma)$ Raman spectra are displayed in (Figure 3). As the samples go from the bottom to the top of the spectrum, their decreased mass, u, rises. In light of this, the $LO(\gamma)$ phonon frequency (~ 208 cm^{-1}) falls from the bottom to the top. Normalization of the peak intensities to one is applied.

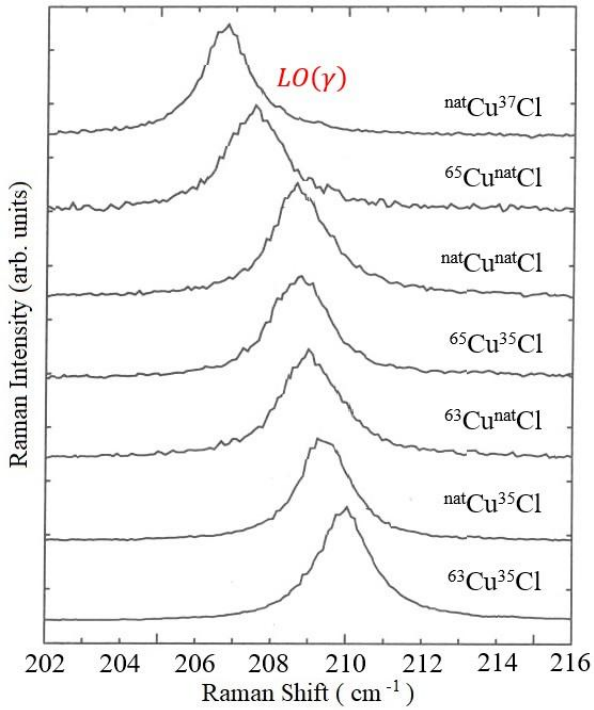

Figure 3. Raman spectra of the isotopically modified CuCl's LO phonon at 2K. As would be predicted for a zone center phonon, $LO(\gamma)$ moves in accordance with $\mu^{-1/2}$ as the lowered mass μ rises from the bottom to the top.

(Figure 4) displays the frequency of $LO(\gamma)$ as a function of the decreased mass. Based on several measurements on the corresponding sample, the mean square deviation is displayed by the error bars. The dashed line represents the lowered mass behavior of the natural chemical in relation to its experimental frequency. The agreement with the optical I point phonon prediction is quite good. For some substances, the full phonon linewidth at half maximum (FWHM) $\Gamma_{LO(\gamma)}$ is reported in Table I along with the experimental $LO(\gamma)$ frequencies. A 0.5 cm^{-1} A wide Gaussian can be used to approximate the spectrometer resolution. A Lorentzian line shape $LO(\gamma)$ [Chen, 2016, P4085, P4087, P] [Zaghloula, 2024, P1] [Menendez, 1984, P2054] is implicitly assumed, and we fit the spectra to a Voigt profile to derive $\Gamma_{LO(\gamma)}$.

***Received**: 02-07-2025 - **Accepted**: 01-09-2025 - **Published**: 10-09-2025*

Alq J Sci. 2025;1(2):157-171
https://doi.org/10.69667/ajs.25205
Alqalam Journal of Science
مجلـــة القلم للعلـوم
https://alqalam.utripoli.edu.ly/index.php/AR

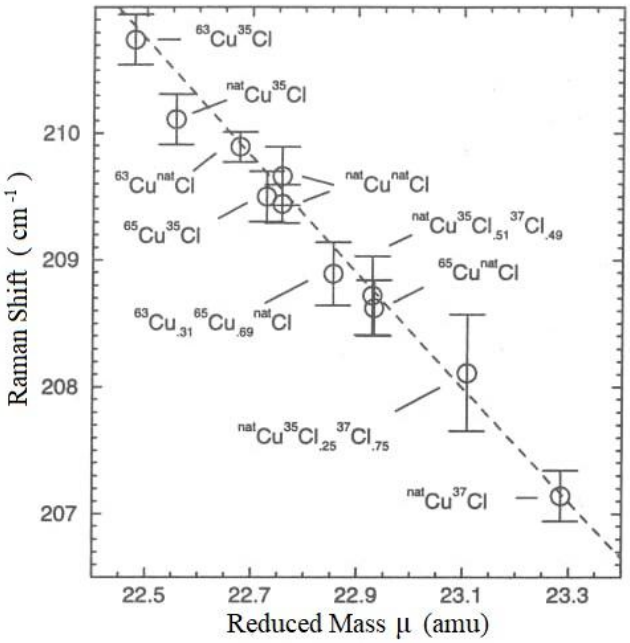

Figure 4: Raman frequencies of the $LO(\gamma)$ phonon at T 5K. Together with a few other isotope mixes, the data match the samples in Table I. The two natural CuCl data points are from separate samples. A lower mass behavior is shown by the solid line.

The Raman spectra of the TO structure exhibit two key features: a narrow peak at 168.5 cm^{-1}, designated as $TO(\gamma)$, and a broad peak at approximately 152.3 cm^{-1}, labeled $TO(\beta)$. These spectra, shown in (Fig. 5), were normalized to the $TO(\gamma)$ peak. They were collected during the same scan as the $LO(\gamma)$ spectra (shown in Fig. 3), though the order of display is different. The vertical bars in the figure mark the average position of the $TO(\gamma)$ peak, based on multiple measurements, and this value is also listed in Table I.

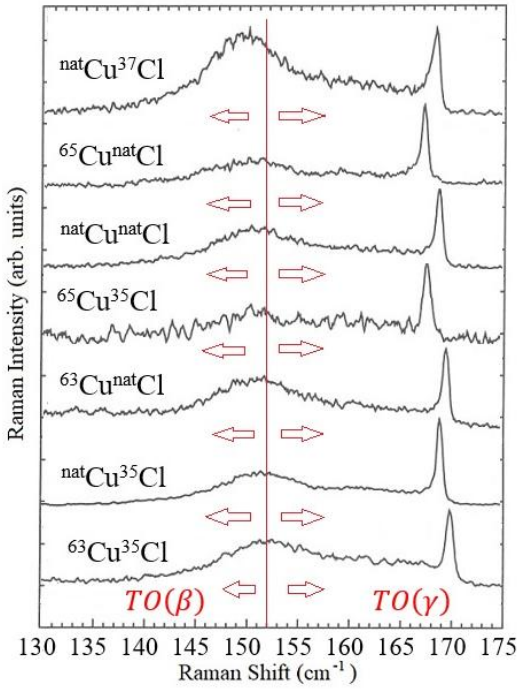

Figure 5. Raman spectra show several isotopically modified CuCl samples' anomalous TO structure. Changes in copper mass cause the $TO(\gamma)$ line to shift rather than changes in μ. When μ changes, the broad $TO(\beta)$ line changes as well.

The $TO(\gamma)$ Raman shift exhibits a pronounced sensitivity to the isotopic mass of copper. Specifically, replacing ^{65}Cu with ^{63}Cu in compounds with chlorine results in a $TO(\gamma)$ shift of 1.6.0±0.6 cm^{-1} as we see in (Fig.6(a)). This shift is significantly larger than the 0.8 cm^{-1} shift predicted by the change in the system's

***Received**: 02-07-2025 - **Accepted**: 01-09-2025 - **Published**: 10-09-2025*

Alq J Sci. 2025;1(2):157-171
https://doi.org/10.69667/ajs.25205
Alqalam Journal of Science
مجلـــة القلم للعلـوم
https://alqalam.utripoli.edu.ly/index.php/AR

reduced mass, μ. Conversely, the $TO(\gamma)$ frequency is less sensitive to the isotopic mass of chlorine. For instance, the substitution of ^{37}Cl with ^{35}Cl leads to a minor $TO(\gamma)$ shift of 0.40±0.5 cm^{-1}, which is substantially smaller than the anticipated shift of 2.1 cm^{-1} derived from the change in reduced mass.

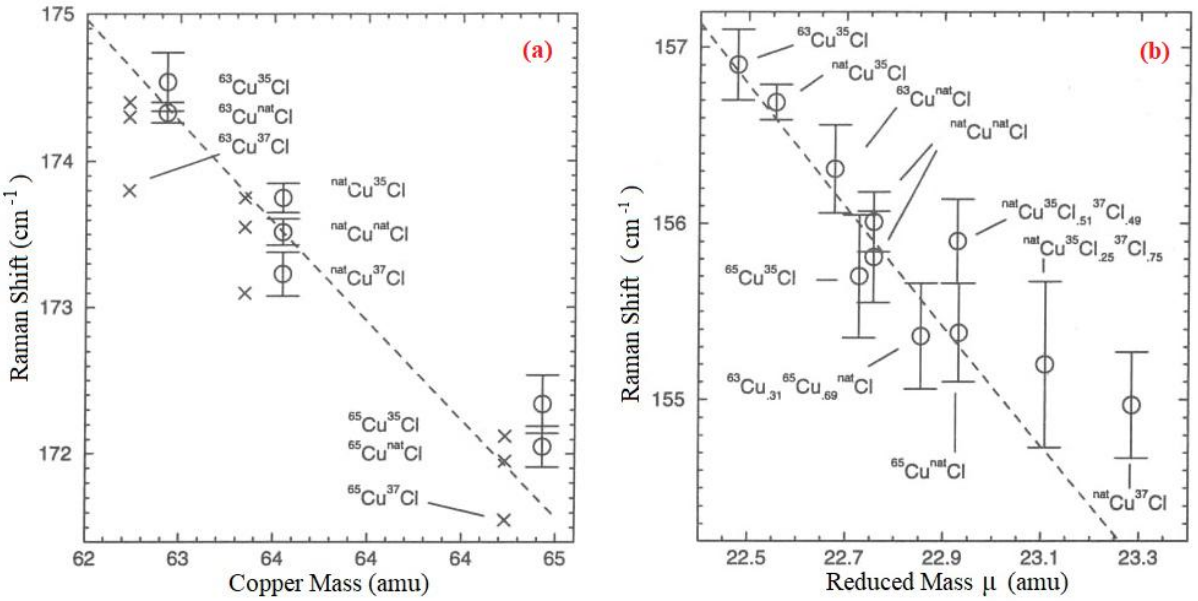

Figure 6: (a) Raman frequencies of the $TO(\gamma)$ peak as a function of the copper mass at 5 K (dashed line $m_{Cu}^{-1/2}$ scaled to the frequency in $^{nat}Cu^{nat}Cl$). The circles are the measured values, and the x are calculated values (Theoretical values). For clarity, the theoretical values have been shifted down by 0.2 amu. The error bars represent the mean square deviation of several measurements. (b) Raman frequencies of the $TO(\beta)$ peak depending on reduced mass at 5 K.

The $TO(\gamma)$ The peak is a narrow feature with a unique line shape that is neither Gaussian nor Lorentzian (see Fig. 2). Spectrometer resolution distorts and broadens the experimental $TO(\gamma)$ peaks shown in (Fig. 5). Therefore, a direct comparison of spectra is only valid if they were measured with the same slit width. To address these challenges, we determined the width of $TO(\gamma)$ by fitting a Gaussian function to the high-frequency side of the peak, starting from the sharp rise on the lower frequency side. We confirmed that the starting point of the fit does not significantly impact the calculated width by testing multiple starting points. The determined values were then corrected for the spectrometer's Gaussian resolution function. The corrected linewidths, $\Gamma_{TO(\gamma)}$, are provided in (Table 2).

Additionally, the $TO(\beta)$ peak changes due to isotope replacement. For certain substances, however, its significant breadth and low intensity make it difficult to detect even small changes in its Raman shift. (Figure 6) (b) shows the average TO(β) frequency shown across the decreased mass based on fitted spectra with a Gaussian profile from many observations in the 130-160 cm^{-1} range, see Table I for more clarification. Moreover, we would like to emphasize that there is no presumption of a reduced mass dependency.

Table 2. The amplitude ratios of $TO(\gamma)$ and $TO(\beta)$, as well as the linewidth $\Gamma_{TO(\gamma)}$ in [cm^{-1}], were measured and computed. The spectrometer resolution is taken into account while adjusting the observed values of $\Gamma_{TO(\gamma)}$. The Fermi resonance model is in good agreement with the trends in the linewidths and the ratios of the amplitudes of $TO(\gamma)$ and $TO(\beta)$. Mean square deviations of many measurements make up the mistakes.

Sample	$\Gamma_{TO(\gamma)}$		$\frac{I(TO(\gamma))}{I(TO(\beta))}$	
	measured	calculated	Measured	calculated
$^{63}Cu^{35}Cl^{(a)}$	0.85	0.84	1.9	2.0
$^{63}Cu^{nat}Cl$	0.71	1.0	2.6	1.8
$^{63}Cu^{37}Cl$	-	1.2	-	0.8
$^{nat}Cu^{35}Cl$	0.59	0.57	2.9	3.1
$^{nat}Cu^{nat}Cl$	0.76	1.1	2.0	1.7
$^{nat}Cu^{37}Cl$	0.9	1.4	1.1	1.0
$^{65}Cu^{35}Cl^{(a)}$	0.8	0.4	3.3	4.5

***Received**: 02-07-2025 - **Accepted**: 01-09-2025 - **Published**: 10-09-2025*

Alq J Sci. 2025;1(2):157-171
https://doi.org/10.69667/ajs.25205
Alqalam Journal of Science
مجلـــة القلم للعلـوم
https://alqalam.utripoli.edu.ly/index.php/AR

$^{65}Cu^{nat}Cl$	0.6	0.63	2.9	3.0
$^{65}Cu^{37}Cl$(b)	-	1.1	-	1.2

(a) The data were taken at T = 5K in this table; samples have different orientations and were grown by a different process. (b) The ^{37}Cl-compound contains about 9% ^{35}Cl.

Here we will only see the key concepts and outcomes of the anharmonic decay of phonons that causes widening and energy shift [Cuscó, 2025, P1], [Menendez, 1984, P2052, P2053]. In the harmonic approximation, the crystal lattice potential is enlarged to quadratic terms in the atomic displacements only, and this is how most lattice dynamical computations are carried out. The quartic and cubic terms in this expansion, however, are frequently non-negligible in a real crystal. Such anharmonicities cause the normal modes to move and broaden as a result of the coupling of the harmonic eigenstates they create. These are described by a complex phonon self-energy

$$\Pi(jq,\omega) = \Delta(jq,\omega) + i\Gamma(jq,\omega) \quad (1)$$

which depends on the frequency ω, phonon wave vector q, and the branch j of the phonon. We consider the renormalization of zone center phonons $(q = \vec{0})$ by anharmonic interaction. For small shifts Δ and broadenings Γ compared to the harmonic Raman frequency, the line shape of the Stokes Raman peak at low temperature $(kT \ll \hbar\omega)$ is

$$Is(j\vec{0},\omega)\, \alpha\, \frac{\Gamma(j\vec{0},\vec{\omega})}{[\omega - \omega_j(\vec{0}) - \Delta(j\vec{0},\omega)]^2 + \Gamma^2(j\vec{0},\omega)} \quad (2)$$

Depending on the study of Raman light scattering, we use the next equation to calculate Raman line broadening [Balkanski, 1983, P1931], [Tallman, 2004, P493]

$$\Gamma(j\vec{0},\omega) = \frac{18\pi}{\hbar^2} \sum_{q,j_1,j_2} \left|(j\vec{0},j_1q_1,j_2q_2)\right|^2 \times [n(j_1q_1) + n(j_2q_2) + 1]\, \delta(\omega_{j1}(q_1) + \omega_{q2}(q_2) - \omega) \quad (3)$$

$V_3(jq,j_1q_1,j_2q_2)$ These are the cubic coefficients in the expansion of the lattice potential in normal coordinates. In the following, we choose the particular case in which a zone center phonon (q = 0) with branch index j decays into two phonons with opposite wave vectors q_1 = q, q_2 = -q and branch indices j_1, j_2, respectively. Conservation of energy is guaranteed by the δ-function in Eq. 3. The number of thermal occupations, $n(jq)$, disappears at low temperatures. Therefore, the right side of Eq. 3 becomes proportional to the two-phonon density of states $\rho_2(\omega)$ if we assume matrix elements V_3 that are constant within the energy range of interest here. The optical Raman frequency $\omega_j(\vec{0})$ may thus be predicted to expand significantly whenever it coincides with a peak in the two-phonon density of states. The assumption may be oversimplified, though, because V_3 It is also dependent on the wave vector of the pair of phonons into which the mode decays. This dependency is provided by [Balkanski, 1983, P1929] [Cusco, 2015, P4, P5] as

$$V_3(j\vec{0},j_1q,j_2\ -q) = \frac{1}{6}\left(\frac{\hbar^3}{8N\omega_j(\vec{0})\omega_{j1}(q)\,\omega_{j2}(-q)}\right)^{\frac{1}{2}} \times \sum_{l',l''} \sum_{K,K',K''} \sum_{\alpha,\beta,\gamma} \Phi_{\alpha,\beta,\gamma}(0,K,l',K',l'',K'') \frac{e_\alpha(K|j\vec{0})\, e_\beta(K'|j_1q)\, (K''|j_2 - q)}{[m_K\, m_{K'}\, m_{K''}]^{\frac{1}{2}}} \times e^{iq.[\vec{R}(l') - \vec{R}(l'')]} \quad (4)$$

where $\Phi_{\alpha,\beta,\gamma}$, is the third derivative of the interatomic potential with respect to displacements along the Cartesian coordinate axes α, β and γ of the atoms (0, κ), (l', κ), and (l'', k') [Menendez, 1984, P2053] [Balkanski, 1983, P1928, P1929]. The index I labels the primitive cell, while denotes the two atoms within the primitive cell. The $e(k|jq)$ are the harmonic eigenvectors. m_k is the atomic mass and N the number of cells in the crystal? We can consider the change of the decay rate with isotope substitution, depending on V_3 .

The anharmonic shift A of a zone-center optical phonon is caused by third-order coupling [Wei, 2021, P3], which represents the decay of one phonon into two phonons. This contrasts with thermal expansion and fourth-order scattering, which cause a frequency-independent shift. The frequency-dependent nature of the third-order coupling can distort the phonon's line shape. Since the anharmonic shift is the real part of the self-energy II (see Eq. 1), it can be calculated from the imaginary part I using a Kramers-Kronig transformation [Pain, 2025, P2, P3].

Received*: 02-07-2025 -* ***Accepted****: 01-09-2025 -* ***Published****: 10-09-2025*

Alq J Sci. 2025;1(2):157-171
https://doi.org/10.69667/ajs.25205
Alqalam Journal of Science
مجلـــة القلم للعلـوم
https://alqalam.utripoli.edu.ly/index.php/AR

In the lattice dynamics part, we can clearly see that the Third-order anharmonic interactions of lattice vibrations are the only basis on which we define a model. Calculating the Raman spectra of CuCl with varying isotopic composition is made possible by it. Only the third-order coupling constant V_3 It is a parameter that can be used. As we know the inelastic neutron scattering is a powerful technique; therefore, it is used to specify CuCl at low temperatures [Gopakumar, 2017, P2, P7, P8], [Prevost, 1977, P3999-P4001]. To determine the phonon dispersion of CuCl, we utilize the parameters that they received from fitting their data to a 14-parameter shell model [Hennion, 1979, P1610, P1621]. The phonon dispersions that were obtained for (full lines) at $^{63}Cu^{nat}Cl$ and dashed lines at $^{65}Cu^{nat}Cl$ are displayed in (Fig. 8 (a)). Using the restriction $q_1 + q_2 = \vec{0}$, the corresponding two-phonon densities of states, $p_2(\omega)$, are displayed in (Fig. 8 (b)). The reduced mass ($\sim 1/\sqrt{\mu}$) determines the optical phonon energies at the zone center, whereas the copper vibrations ($\sim 1/\sqrt{m_{Cu}}$) define the energies of the acoustic branches surrounding the X and K points (Fig. 8 (a)).

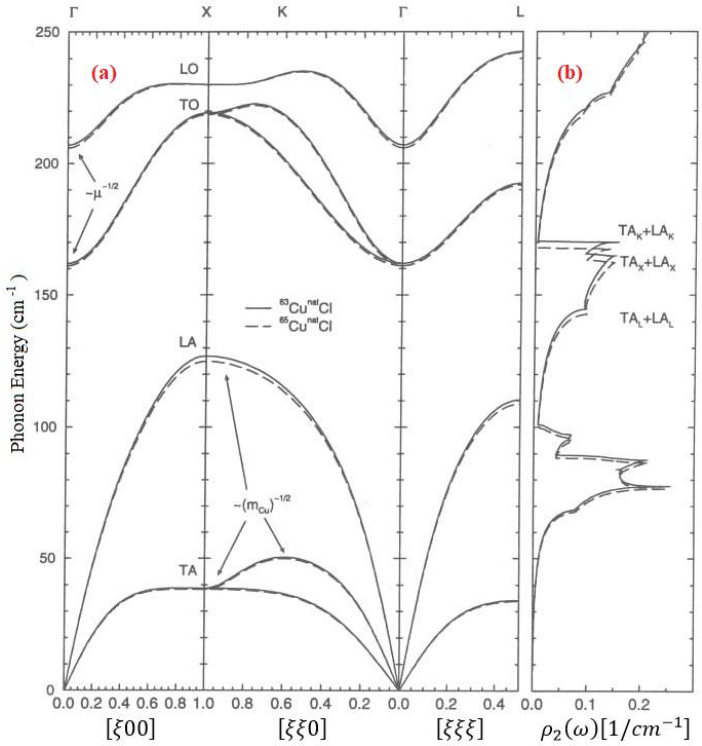

Figure 8. a) CuCl phonon dispersion in high symmetry directions, calculated with the parameters of the shell model. b) The density of states $\vec{p}_2(\omega)$ with two phonons. There are indications for the branch combinations that produce Van Hove singularities in the TO energy range

It is possible to deduce from Patel and Sherman's findings that the dominance of the copper eigenvectors is more than merely a characteristic of the shell model parameterization. When these scientists examined the eigenvector q-dependence of CuCl phonons from a rigid-ion model to those from the shell model, they discovered that there was only a little difference between the two models [Patel, 1990, P923].

Using an 8240-point mesh and an energy resolution of 0.1 cm^{-1}, the two-phonon density of states (DOS) in CuCl was determined. Two notable peaks were found in this calculation close to the harmonic TO frequency (~162 cm^{-1}); these are Van Hove singularities that arise from combinations of the longitudinal acoustic (LA) and transverse acoustic (TA) branches at the Brillouin zone's X and K points.

The two-phonon combination band peaks could only be found to a minimal extent because of the low precision of neutron tests (6% for phonon frequencies). In order to reduce artifacts in the calculated spectra, the two-phonon DOS was smoothed and approximated by averaging across a width of 1.5 cm^{-1}. The flat TA branches in CuCl are responsible for the rapid decrease of about 168 cm^{-1}, which is the most noticeable aspect of the smoothed spectrum. The smoothing technique has little effect on this distinctive dip, which is strong.

It was discovered that the two-phonon DOS is directly proportional to the phonon self-energy broadening (Γ), which was calculated under the assumption of a q-independent matrix element. After that, a Kramers-Kronig transformation was used to determine the actual part of the self-energy (Δ). These approximations were used in the calculation of the Raman spectra in the TO region. The unrenormalized TO frequency

Received: *02-07-2025* - ***Accepted***: *01-09-2025* - ***Published***: *10-09-2025*

Alq J Sci. 2025;1(2):157-171
https://doi.org/10.69667/ajs.25205
Alqalam Journal of Science
مجلـــة القلم للعلـوم
https://alqalam.utripoli.edu.ly/index.php/AR

crossing the actual part of the self-energy explains the two peaks in the spectrum. In order to fit the experimentally obtained spectrum, model spectra were calculated with different coupling constants. Higher coupling constants result in bigger amplitudes of Δ relative to Γ and also increase the distance between the real component of the self-energy and the unrenormalized TO frequency. Even though the simulated peak frequency is somewhat higher than the real value, the best-fit simulation offers a decent approximation of the observed line form.

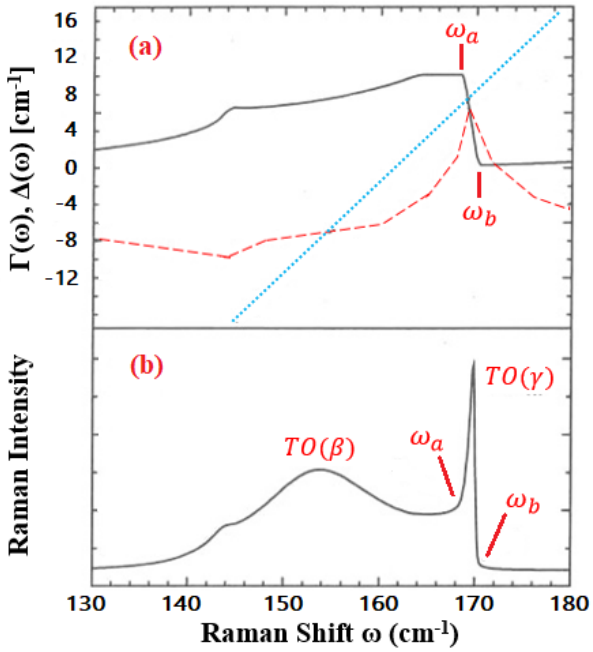

Figure 9. Fermi resonance model for CuCl's TO anomaly. (a) $\Gamma(\omega) = V_3^2\vec{p}_2(\omega)$ is the imaginary component of the phonon self-energy, shown by the solid line. $\Delta(\omega)$, a Kramers-Kronig related quantity, is shown by the dashed red line. For $TO(0,j)$, the dotted straight blue line is introduced $\omega - \omega_{TO}(\vec{0})$. (b) The intensity is provided in arbitrary units for the simulated $^{nat}Cu^{nat}Cl$ spectrum

We now want to talk about the main issue of consistency in the described process: The phonon dispersion of CuCl was measured using inelastic neutron scattering, which measures phonons that had already been renormalized by the anharmonic interaction. The unrenormalized harmonic frequencies are not obtained by parameterizing the harmonic shell model with these values [Hennion, 1979, P1616]. However, we implicitly employed the phonon dispersion as if it were unrenormalized in our computation of the complex self-energy $\sum(j\vec{0},\omega)$. Therefore, it is expected that the absolute phonon frequencies determined by using the anharmonic renormalization will differ from those being observed. In addition, we have overlooked the fourth-order contributions to the real part of the self-energy and thermal expansion, which also cause a line shift and could explain the discrepancy between the calculations and measurements. The location of the drop in $\vec{p}_2(\omega)$ and the harmonic frequency $\omega_{TO}(\vec{0})$ would not be known with precision, even if the renormalization issue did not occur. It is assumed that both come from a fit of the phonon dispersion to the shell model, which may not accurately recreate the phonon frequencies at every Brillouin zone location. However, this consistency issue has minimal impact on the relative shifts brought about by the isotope effect.
Additionally, we have considered the lattice dynamics within the framework of the virtual crystal approximation, hence ignoring the consequences of isotope disorder in our mathematical calculations. To project the masses of the ions on the cation or anion sublattice, an average over the relevant isotopic composition is used. As the reported disorder effects are already very minor for germanium (Ge) [Göbel, 1997, P216] or stannum (Sn) [Sharma, 2020, P1044], where the mass variance parameters $g(k)$ are about an order of magnitude smaller, shifts in the Raman spectra of CuCl caused by isotope disorder should be insignificant. Both isotopically pure and isotopically 118 disordered materials show good agreement between the measured $LO(\gamma)$ frequencies and the expected decreased mass behavior, which further supports the virtual crystal approach (Fig. 4). On the other hand, the linewidth of $LO(\gamma)$ varies little with isotope disorder. The TO zone center phonon is even less affected by isotope disorder-induced scattering because, as Fig. 8 illustrates, the optical branches of the phonon dispersion bend monotonically upward. Consequently, the ensuing self-energy is tightly suppressed, and there is only a small one-phonon density of states to scatter

Received: *02-07-2025* - ***Accepted***: *01-09-2025* - ***Published***: *10-09-2025*

Alq J Sci. 2025;1(2):157-171
https://doi.org/10.69667/ajs.25205
Alqalam Journal of Science
مجلـــة القلم للعلـوم
https://alqalam.utripoli.edu.ly/index.php/AR

into. Our estimates also did not account for the effects of structural disorder, where ions would be found on off-center locations.

To calculate the phonon dispersion of CuCl, we simply change the atomic masses m_k. It is anticipated that the force constants of the shell model would remain unaffected by the isotope replacement. As previously mentioned, the two-phonon density of states $p_2(\omega)$ is computed for each isotopic composition to determine the line broadening $\Gamma(j\vec{0},\omega)$ and the line shift $\Delta(j\vec{0},\omega)$. We calculate the Raman spectra for different isotopic compositions using the same anharmonic coupling value $V_3^2 = 70\ cm^{-2}$ in each case, and the associated harmonic frequency $\omega_{TO}(\vec{0})$. We find that the $TO(\gamma)$ frequencies are similar for compounds that have the same mass of copper. Within these groups, $TO(\gamma)$ shifts follow the pattern indicated by the lowered masses, meaning that the molecule with the lighter chlorine isotope has a greater $TO(\gamma)$ energy. The energies of $TO(\gamma)$ changed by +3.1 cm^{-1} for the aforementioned causes are shown by the crosses in (Fig. 6 (a)).

We discovered that the data and our estimated isotope shifts agreed rather well. With our method, the complex modifications in the TO structure brought about by the isotope replacement-induced variations in eigenvectors and phonon frequencies are automatically taken into consideration. The results may be summed up as follows: The location of the $TO(\gamma)$ The phonon is mostly determined by the abrupt decrease in the imaginary component of the self-energy Γ, as can be seen in Fig. 9. This drop is caused by a Van Hove singularity of TA + LA acoustic band combinations concerning the X and K positions. The decrease shifts mainly for Cu isotope substitution because copper ions are the main component of these modes. As far as we know, the $TO(\gamma)$ peaks of compounds with the same mass of copper form groups because the substitution of chlorine does not alter the decrease in Γ. $\omega - \omega_{TO}(\vec{0}) = \Delta(j\vec{0},\omega)$, or the position in Fig. 9 (a) where the straight line is closest to the dotted line that signifies Δ, is the second prerequisite for the $TO(\gamma)$ placement inside these groups. When the chlorine mass in compounds with the same copper mass is modified, the whole isotope impact on the reduced mass shifts the straight line in Fig. 9 (a). As the chlorine masses get smaller, the straight line and the point where it crosses or is closest to Δ both shift to higher frequencies. However, the strong slope of the real component of the self-energy Delta in this energy range means that the shift of this point is not as large as a decreased mass shift would imply.

The measured linewidths of the $TO(\gamma)$ The peak for compounds made from native copper increases with increasing chlorine mass (Table II). Our calculated spectra confirm this, as seen in (Fig. 9): The frequencies $\omega_a$and ω_b point to the lower and upper borders of the drop in Γ, respectively. If the copper mass remains constant, these frequencies ought to remain constant since the acoustic vibrations involved have a primary copper nature. In Fig. 9 (b), the edges of $\vec{\rho}_2(\omega)$ at $\omega_a$and ω_b are plainly visible in the spectrum. Consequently, the linewidth $\Gamma_{TO(\gamma)}$ is essentially determined by the amplitude of the spectrum between $\omega_a$and ω_b. The lowest values of $[\omega - \omega_{TO}(\vec{0}) - \Delta(j\vec{0},\omega)]$ yield the highest amplitude. Ignoring this value with respect to Γ, we see that Eq. 2 simplifies to $I \sim \Gamma^{-1}$. As the mass of chlorine grows, the dotted line in Fig. 9 (a) moves towards lower frequencies, Γ therefore rises. As the resultant spectrum's linewidth increases, its amplitude lowers. Nevertheless, a quantitative comparison between the estimated and real linewidths $\Gamma_{TO(\gamma)}$ is not possible due to the limited spectrometer resolution. While the larger predicted linewidths, up to 1.6 cm^{-1}, would remain mostly unaltered, the 0.5 cm^{-1} spectrometer resolution would greatly expand the least calculated linewidth, which is around 0.4 cm^{-1}. Furthermore, the linewidth $\Gamma_{TO(\gamma)}$ is determined by the finer characteristics of the two-phonon density of states between ω_a and ω_b. We find that theory and experiment agree rather well for both the absolute values of $\Gamma_{TO(\gamma)}$ and the trends with isotope replacement, despite these two uncertainties.

The Fermi resonance model generally matches experimental $TO(\gamma)/\ TO(\beta)$ amplitude ratios (Table II), except for $^{65}Cu^{35}Cl$, where the predicted ratio is too high. $TO(\beta$Frequencies are ~1.7 cm^{-1} lower than measured but show isotope shifts proportional to reduced mass (Figs. 6 (b), 9). Chlorine substitution mainly shifts $[\omega - \omega_{TO}(\vec{0})]$ with minimal Δ change, producing reduced-mass behavior; copper substitution shifts both, but the $TO(\beta)$ peak still follows reduced-mass trends, consistent with Fig. 6 (b).

We model $LO(\gamma)$ behavior using a reduced mass approach similar to the TO case. Two LA modes near the L point dominate the two-phonon DOS around $LO(\gamma)$, approximated with an average acoustic frequency of 105 cm^{-1}. From Eq. 4, $(V_3^{LO})^2$ = 26 cm^{-2} yields linewidths ~1.6 cm^{-1}, matching observations (Table I). The measured $LO(\gamma)$ frequency is ~6 cm^{-1} higher than calculated, and simulated $I[LO(\gamma)]/I[(TO(\gamma)]$ ratios are up to 4× larger than measured. Isotope substitution changes $(V_3^{LO})^2$ by < 5%, giving predicted linewidth variations < 0.08 cm^{-1}—much smaller than observed, suggesting disorder-induced elastic scattering.

In this model, isotope broadening is proportional to the DOS projected on each sublattice and weighted by its mass-variance parameter. For samples made under the same conditions, $^{nat}Cu^{35}Cl$ shows the smallest linewidth ($\Gamma_{LO(\gamma)}$= 1.34 cm^{-1}) and lowest disorder ($g_{tot} = 0.7 \times 10^{-4}$). Switching to $^{nat}Cu^{37}Cl$ increases g_{tot} by ~2.9 × 10^{-4} and linewidth by ~0.14 cm^{-1}. Other isotopic compositions have g_{tot} ≈ (5.1–5.8) × 10^{-4} and linewidths of $\Gamma_{LO(\gamma)}$ = 1.64–1.75 cm^{-1}, about 0.38 cm^{-1} higher than $^{nat}Cu^{35}Cl$.

Received: *02-07-2025* - ***Accepted***: *01-09-2025* - ***Published***: *10-09-2025*

Alq J Sci. 2025;1(2):157-171
https://doi.org/10.69667/ajs.25205
Alqalam Journal of Science
مجلـــة القلم للعلـوم
https://alqalam.utripoli.edu.ly/index.php/AR

Conclusion

In this study, we could investigate the Raman spectra of copper(I) chloride (CuCl) samples with varying isotopic compositions at low temperature (T=5K) to understand the effects of isotope disorder on phonon linewidths. Our findings are consistent with the Fermi resonance model, which provides a robust explanation for the anomalous Raman spectra of CuCl. Our results confirm that the observed variations in the linewidths of the $TO(\gamma)$ phonon are qualitatively consistent with a broadening caused by isotope disorder, specifically the mass-variance parameter $g(k)$. While a quantitative analysis would necessitate a spectrometer with higher resolution, the qualitative agreement supports this mechanism. We found that the $TO(\gamma)$ peak's position is closely tied to the edge of the two-phonon density of states, which is a consequence of Van Hove singularities. Since these singularities arise mainly from acoustic dispersion branches involving copper vibrations, the $TO(\gamma)$ peak exhibits a copper-dominated isotope effect. For samples with a natural copper abundance, the linewidth of the $TO(\gamma)$ peak increases with increasing chlorine mass. The frequency changes of the $TO(\beta)$ peak, however, are consistent with a reduced-mass-like behavior, as predicted by the Fermi resonance model. Furthermore, the ratio of the peak intensities of $TO(\gamma)$ to $TO(\beta)$ decreases with increasing chlorine mass. The LO phonon, on the other hand, interacts with a relatively flat two-phonon density of states. Its position shifts in a manner consistent with a normal zone-center phonon, following a decreased mass behavior. The linewidth of the $LO(\gamma)$ phonon is attributed to a combination of anharmonic and isotope-disorder-induced broadening. We were able to account for all experimental observations using a single effective anharmonic coupling parameter V_3. In contrast to our findings, off-center models fail to account for the Raman data. An early quantitative description of such a model, which implies two reduced-mass-like oscillators, cannot explain the differing mass dependences of the $TO(\gamma)$ and $TO(\beta)$ phonons. While we cannot definitively rule out the presence of off-center defects in CuCl, they are neither necessary nor sufficient to explain the observed Raman anomaly. An interesting exception was the $^{63}Cu^{35}Cl$ samples, which showed anomalously high $LO(\gamma)$ linewidths despite their vanishing mass-variance parameter. This discrepancy may be attributed to a lower sample quality, surface effects, or compositional differences resulting from a different manufacturing batch. Future research could investigate these possibilities to ensure sample consistency across different compositions.

Conflict of interest. Nil

References

1. Alhaddad T, Shoker MB, Pagès O, Polian A, Torres VJB, Godec YL, et al. Taxonomy of high pressure vibration spectra of zincblende semiconductor alloys based on the percolation model. Sci Rep. 2025;15:1212.
2. Aree T, McMonagle CJ, Michalchuk AAL, Chernyshov D. Low-frequency lattice vibrations from atomic displacement parameters of a-FOX-7, a high energy density material. Acta Crystallogr B Struct Sci Cryst Eng Mater. 2022;78(Pt 3):376-84.
3. Asen-Palmer M, Bartkowski K, Gmelin E, Cardona M, Zhernov AP, Inyushkin AV, et al. Thermal conductivity of germanium crystals with different isotopic compositions. Phys Rev B Condens Matter. 1997;56(15):9431-47.
4. Balkanski M, Wallis RF, Haro E. Anharmonic effects in light scattering due to optical phonons in silicon. Phys Rev B Condens Matter. 1983;28(4):1928-34.
5. Behera S, Samsur Sk. Hybridization of the Two-Phonon Bound State with the Local Mode in imperfect crystals. J Phys Colloques. 1981;42(C6):C6-528-C6-30.
6. Boyce JB, Hayes TM, Mikkelsen JC Jr, Stutius W. EXAFS investigation of superionic conduction in CuI. Solid State Commun. 1980;33(2):183-9.
7. Bud'ko SL, Lapertot G, Petrovic C, Cunningham CE, Anderson N, Canfield PC. Boron isotope effect in superconducting MgB2. Phys Rev Lett. 2001;86(9):1877-80.
8. Castillo-Quevedo C, Cabellos JL, Aceves R, Núñez-González R, Posada-Amarillas A. Cu-Doped KCl Unfolded Band Structure and Optical Properties Studied by DFT Calculations. Materials (Basel). 2020;13(19):4300.
9. Cheng F, Liu Y, Ma Z, Al Hossainb MS, Somer M. The isotope effect of boron on the carbon doping and critical current density of Mg11B2 superconductors. J Mater Chem C Mater. 2017;5:663-8.
10. Chen Y, Dai L. Automated decomposition algorithm for Raman spectra based on a Voigt line profile model. Appl Opt. 2016;55(15):4085-94.
11. Cusco R, Domenech-Amador N, Novikov S, Foxon CT, Artus L. Anharmonic phonon decay in cubic GaN. Phys Rev B Condens Matter Mater Phys. 2015;92(7):075206.
12. Cuscó R, Taguchi A, Yamaguchi T. Phonon anharmonicity in α-In2O3: A Raman scattering study of the A1g modes. J Alloys Compd. 2025;1020:179350.
13. Fukumoto T, Nakashima S, Tabuchi K, Mitsuishi A. Temperature Dependence of Raman Spectra of Cuprous Halides. Phys Status Solidi B. 1976;73(1):341-8.
14. Gopakumar AM, Gupta MK, Mittal R, Rols S, Chaplot SL. Investigating Anomalous Thermal Expansion of Copper Halides by Inelastic Neutron Scattering and Abinito Phonon Calculations. Phys Chem Chem Phys. 2017;19(18):12107-16.

Received*: 02-07-2025 -* ***Accepted****: 01-09-2025 -* ***Published****: 10-09-2025*

Alq J Sci. 2025;1(2):157-171
https://doi.org/10.69667/ajs.25205
Alqalam Journal of Science
مجلـــة القلم للعلـوم
https://alqalam.utripoli.edu.ly/index.php/AR

15. Göbel A, Ruf T, Cardona M, Lin CT, Merle JC. Comment on "Ground State Structural Anomalies in Cuprous Halides: CuCl". Phys Rev Lett. 1996;77(12):2591.
16. Göbel A, Ruf T, Lin CT, Cardona M, Merle JC, Joucla M. Effects of isotopic composition on the lattice dynamics of CuCl. Phys Rev B Condens Matter. 1997;56(1):210-22.
17. Gweon GH, Sasagawa T, Zhou SY, Graf J, Takagi H, Lee DH, et al. An unusual isotope effect in a high-transition-temperature superconductor. Nature. 2004;430(6996):187-90.
18. Hattori K, Tsunetsugu H. Strong coupling superconductivity mediated by three-dimensional anharmonic phonons. Phys Rev B Condens Matter Mater Phys. 2010;81(13):134503.
19. Hennion B, Prevot B, Krauzman M, Pick RM, Dorner B. Neutron scattering of the TO phonon in CuCl at 5K. J Phys C Solid State Phys. 1979;12(9):1609.
20. Hodges PJ, Ross AJ, Crozet P, Salami H, Brown JM. On the Spin-Orbit Splitting of CuCl2 in its 2Πg Ground State. J Chem Phys. 2007;127(2):024309.
21. Hodovanets H, Ran S, Canfield PC, Bud'ko SL. Boron isotope effect in single crystals of superconductor. Philos Mag. 2013;93(14):1748-54.
22. Kragh H. The isotope effect: Prediction, discussion, and discovery. Stud Hist Philos Sci B Stud Hist Philos Mod Phys. 2012;43(3):176-83.
23. Krauzman M, Pick RM, Poulet H, Hamel G, Prevot B. Raman Detection of One-Phonon—Two-Phonon Interactions in CuCl. Phys Rev Lett. 1974;33(9):528-31.
24. Lan T, Li CW, Niedziela JL, Smith H, Abernathy DL, Rossman GR, et al. Anharmonic lattice dynamics of Ag2O studied by inelastic neutron scattering and first-principles molecular dynamics simulations. Phys Rev B Condens Matter Mater Phys. 2014;89(5):054306.
25. Lefkowitz I, Manning JS, Bloomfield PE. Diamagnetic transition in disordered CuCl. Phys Rev B Condens Matter. 1979;20(11):4506-15.
26. Lindsay L, Broido DA, Reinecke TL. Phonon-isotope scattering and thermal conductivity in materials with a large isotope effect: A first-principles study. Phys Rev B Condens Matter Mater Phys. 2013;88(14):144306.
27. Lin ML, Miscuglio M, Polovitsyn A, Leng YC, Martín-García B, Moreels I, et al. Giant-Shell CdSe/CdS Nanocrystals: Exciton Coupling to Shell Phonons Investigated by Resonant Raman Spectroscopy. J Phys Chem Lett. 2019;10(3):399-405.
28. Majzlan J, Herrmann J, Števkob M, Wiederhold JG, Lazarov M, Milovský R. Isotope diffusion and re-equilibration of copper and evaporation of mercury during weathering of tetrahedrite in an oxidation zone. Geochemistry. 2023;83(2):126019.
29. Menendez J, Cardona M. Temperature dependence of the first-order Raman scattering by phonons in Si, Ge, and a-Sn: Anharmonic effects. Phys Rev B Condens Matter. 1984;29(4):2051-61.
30. Ono S. Phase transition in ZnSe at high pressures and high temperatures. J Phys Chem Solids. 2020;141:109409.
31. Pain JC, Tacu M. Imaginary part of the conductivity using Kramers-Kronig relations. arXiv:250614941v1 [physicsplasm-ph]. 2025.
32. Pang HJ, Yu H, Li WJ, Chen LC, Qiu PF, Chen XJ. High-order phonon anharmonicity in Yb-filled skutterudites. Phys Rev B. 2024;109(4):045202.
33. Park CH, Chadi DJ. Ground State Structural Anomalies in Cuprous Halides: CuCl. Phys Rev Lett. 1996;76(13):2314-7.
34. Park CH, Chadi DJ. Park and Chadi Reply. Phys Rev Lett. 1996;77(12):2592.
35. Patel C, Sherman WF. Eigenvalues And Eigenvectors IN CuCI at 4.2 K. Physica B. 1990;165-166:923-4.
36. Pham TN, Hamamoto Y, Inagaki K, Son DN, Hamada I, Morikawa Y. Insight into Trimeric Formation of Nitric Oxide on Cu(111): A Density Functional Theory Study. J Phys Chem C. 2020;124(5):2968-77.
37. Phillips JC. Ionicity of the Chemical Bond in Crystals. Rev Mod Phys. 1970;42(3):317-56.
38. Potts JE, Hanson RC, Walker CT, Schwab C. Temperature dependence of the Raman scattering from CuCl. Phys Rev B Condens Matter. 1974;9(6):2711-6.
39. Prevot B, Hennion B, Dorner B. Phonon spectrum of CuCl at 4.2K and its temperature dependence. J Phys C Solid State Phys. 1977;10(20):3999.
40. Ruvalds J, Zawadowski A. Two-Phonon Resonances and Hybridization of the Resonance with Single-Phonon States. Phys Rev B Solid State. 1970;2(4):1172-82.
41. Sakata M, Hoshino S, Harada J. Neutron diffraction study of asymmetric anharmonic vibration of the copper atom in cuprous chloride. Acta Crystallogr A. 1974;30(5):655-61.
42. Schneider JW, Kiefl RF, Chow K, Cox SFJ, Dodds SA, DuVarney RC, et al. Local Tunneling and Metastability of Muonium in CuCl. Phys Rev Lett. 1992;68(21):3172-5.
43. Schreurs J, Mueller MH, Schwartz LH. Neutron diffraction study of partial radial densities in γ-CuCl, including an appendix on the effect of instrumental resolution on radial density analysis. Acta Crystallogr A. 1976;32(4):618-26.
44. Sekkal W, Aourag H, Certier M. Molecular dynamics simulation of high pressure phases of CuCl and CuBr. J Phys Chem Solids. 1998;59(8):1293-301.
45. Serrano J, Cardona M, Ritter TM, Weinstein BA, Rubio A, Lin CT. Pressure and temperature dependence of the Raman phonons in isotopic g-CuI. Phys Rev B Condens Matter Mater Phys. 2002;66(24):245202.

Received: *02-07-2025* - ***Accepted***: *01-09-2025* - ***Published***: *10-09-2025*

Alq J Sci. 2025;1(2):157-171
https://doi.org/10.69667/ajs.25205
Alqalam Journal of Science
مجلـــة القلم للعلـوم
https://alqalam.utripoli.edu.ly/index.php/AR

46. Shand ML, Hochheirner HD, Krauzman M, Potts JE, Hanson RC, Walker CT. Experimental and theoretical study of the anomalous Raman spectrum in the transverse optic phonon region of CuCl. Phys Rev B Condens Matter. 1976;14(10):4637-46.
47. Sharma A, Abdur Rahim, Kim D, Tripathi AK, Singh S, Lee J, et al. Effect of Ge doping on the electrical properties of amorphous Zn–Sn–O thin films. Curr Appl Phys. 2020;20(9):1041-8.
48. Stegemann F, Stahl J, Bartsch M, Zacharias H, Johrendt D, Janka O. Temperature Induced Valence Phase Transition in Intermediate-Valent YbPd2Al3. Chem Sci. 2019;10(48):11086-94.
49. Tallman RE, Ritter TM, Weinstein BA, Cantarero A, Serrano J, Lauck R, et al. Pressure measurements of TO-phonon anharmonicity in isotopic ZnS. Phys Status Solidi B. 2004;241(3):491-4.
50. Ulrich C, Göbel A, Syassen K, Cardona M. Pressure-Induced Disappearance of the Raman Anomaly in CuCl. Phys Rev Lett. 1999;82(2):351-4.
51. Vaccari M, Grisenti R, Fornasini P, Rocca F, Sanson A. Negative thermal expansion in CuCl: An extended x-ray absorption fine structure study. Phys Rev B Condens Matter Mater Phys. 2007;75(18):184307.
52. Varshney D, Jain S, Shriya S, Khenata R. High-pressure and temperature-induced structural, elastic, and thermodynamical properties of strontium chalcogenides. J Theor Appl Phys. 2016;10:183-93.
53. Wang ZH, Chen XY, Zhang Z, Zhang X, Wei SH. Profiling the off-center atomic displacements in CuCl at finite temperatures with a deep-learning potential. Phys Rev Mater. 2023;7(3):034601.
54. Watanabe H, Nebel CE, Shikata S. Isotopic Homojunction Band Engineering from Diamond. Science. 2009;324(5933):1425-8.
55. Wei B, Sun Q, Li C, Hong J. Phonon anharmonicity: a pertinent review of recent progress and perspective. Sci China Phys Mech Astron. 2021;64(11):117001.
56. Wei SH, Zhang SB, Zunger A. Off-Center Atomic Displacements in Zinc-Blende Semiconductor. Phys Rev Lett. 1993;70(11):1639-42.
57. Yu Y, Turkowski V, Hachtel JA, Puretzky AA, Ievlev AV, Din NU, et al. Anomalous isotope effect on the optical bandgap in a monolayer transition metal dichalcogenide semiconductor. Sci Adv. 2024;10(8):eadj0758.
58. Zaghloula MR, Le Bourlotb J. A highly efficient Voigt program for line profile computation. J Quant Spectrosc Radiat Transf. 2025;330:109234.
59. Zhang JM, Ruf T, Cardona M. Raman spectra of isotopic GaN. Phys Rev B Condens Matter. 1997;56(23):14399-406.
60. Zhang JM, Ruf T, Lauck R, Cardona M. Isotope effects on exciton energies in CdS. Phys Rev B Condens Matter Mater Phys. 1998;57(16):9716-22

Received: *02-07-2025* - ***Accepted***: *01-09-2025* - ***Published***: *10-09-2025*